

PCCP

Accepted Manuscript



This is an *Accepted Manuscript*, which has been through the Royal Society of Chemistry peer review process and has been accepted for publication.

Accepted Manuscripts are published online shortly after acceptance, before technical editing, formatting and proof reading. Using this free service, authors can make their results available to the community, in citable form, before we publish the edited article. We will replace this *Accepted Manuscript* with the edited and formatted *Advance Article* as soon as it is available.

You can find more information about *Accepted Manuscripts* in the [Information for Authors](#).

Please note that technical editing may introduce minor changes to the text and/or graphics, which may alter content. The journal's standard [Terms & Conditions](#) and the [Ethical guidelines](#) still apply. In no event shall the Royal Society of Chemistry be held responsible for any errors or omissions in this *Accepted Manuscript* or any consequences arising from the use of any information it contains.

Quantum Chemical and Matrix-IR Characterization of $\text{CH}_3\text{CN}-\text{BCl}_3$: A Complex with Two Distinct Minima Along the B-N Bond Potential

John P. Wrass¹, Daniel Sadowsky^{2,3}, Kaitlin M. Bloomgren,¹
Christopher J. Cramer² and James A. Phillips^{1,*}

* Author to whom correspondence should be addressed:

email: phillija@uwec.edu

phone: 715-864-3938

fax: 715-836-4979

1) Department of Chemistry
University of Wisconsin Eau-Claire
Eau Claire, WI 54702

2) Department of Chemistry, Chemical Theory Center, and Supercomputing
Institute
University of Minnesota
Minneapolis, MN 55455

3) Institute of Biogeochemistry and Pollutant Dynamics
ETH Zurich
8092 Zurich, Switzerland

ABSTRACT:

We have characterized the structural and energetic properties of $\text{CH}_3\text{CN}-\text{BCl}_3$ via computations and matrix-IR spectroscopy. We find two equilibrium structures of the complex via computations. At the MP2/aug-cc-pVTZ level, the global minimum energy structure has a B-N distance of 1.601 Å, and a binding energy of 12.0 kcal/mol. The secondary structure lies 7.1 kcal/mol higher in energy with a B-N distance of 2.687 Å and a binding energy of 4.9 kcal/mol. Computational scans of the B-N potential curve using both DFT and post-HF methods indicate that a significant barrier exists between these structures, and that it lies 1 to 2 kcal/mol above the secondary minimum at a B-N distance of about 2.2 Å. We also observed several key, structurally-sensitive IR bands for six isotopic forms of the complex in neon matrices, including: The B-Cl asymmetric stretching band (ν_{BCl}^a) at 792 cm^{-1} and the C-N stretching band (ν_{CN}) at 2380 cm^{-1} (for the primary isotopomer, $\text{CH}_3\text{C}^{14}\text{N}-^{11}\text{BCl}_3$). These frequencies are consistent with computational predictions for the minimum-energy form of the complex. Energy decomposition analyses were conducted for $\text{CH}_3\text{CN}-\text{BCl}_3$ and also two related complexes, $\text{CH}_3\text{CN}-\text{BF}_3$ and $\text{CH}_3\text{CN}-\text{BH}_3$. These provide insight into the trend in Lewis acidity of the BX_3 acceptors toward nitriles. Furthermore, these analyses indicate that the barrier along the B-N potential of $\text{CH}_3\text{CN}-\text{BCl}_3$ results from Pauli repulsion between the π electrons on the nitrile moiety and the chlorine atoms in BCl_3 , which is significant at relatively long distances where attractive bonding interactions fail to overcome it.

Introduction

Spectroscopic investigations of donor-acceptor complexes continue to be an active area of study.¹ Furthermore, there is special interest in the energetic properties of these systems that stems from their role as benchmarks for the validation of new computational methodologies.² Within this broader context, a great deal of our work has been directed toward the properties of nitrile-boron trifluoride complexes.³⁻⁹ One of the most peculiar features of these systems is the degree to which their structures can change markedly between the gas phase and condensed-phase media.⁶⁻¹⁰ The most direct illustrations of these changes come from comparisons between experimental gas-phase and solid-state structures.^{10,11} For example, the gas-phase (microwave) structure of CH₃CN–BF₃ has a B-N distance of 2.01 Å,¹² while the crystal structure exhibits a B-N distance of 1.63 Å.¹³

Subsequent to these direct structural determinations, we found that the intermolecular potential of CH₃CN–BF₃ is quite flat along the B-N bond coordinate,^{4,8} and that this was the key feature underlying the medium effects on the structural properties of this system.⁸ In turn, we subsequently demonstrated that a large-amplitude motion along the B-N coordinate manifested a genuine discrepancy between the experimental (vibrationally-averaged) and theoretical (equilibrium) structures.⁸ From an experimental standpoint, we found via frequency shifts that the structure of CH₃CN–BF₃ varied systematically across a range of bulk, inert, condensed-phase media, including Ar, N₂, and Ne matrices, indicating that an increase in charge-stabilizing ability of the medium leads to a compression of the B-N bond.^{3,7} Ultimately, using the Polarized Continuum Model (PCM)¹⁴ to represent the solvation effects of these inert media, we were able to

rationalize the trends across this series and further illustrate the effects on the B-N bond potential and the overall structure of the complex.⁸

In studies of related systems, we found that changes in the substituent on the nitrile moiety significantly affected the overall medium sensitivity of the resulting complexes.^{5,6,9} In general, the medium effects are greatest with weaker bases, since the gas-phase complexes are more weakly bonded, and in turn, there is more potential to compress the B-N bond in condensed phases. For example, extremely large gas-solid structure differences have been observed for HCN-BF₃,¹¹ and, in turn, were predicted for the singly-halogenated analogs of CH₃CN-BF₃ (XCH₂CN-BF₃; X=F,Cl).⁶ In these systems, the differences between the B-N distances of the gas-phase and solid-state complexes approach 0.8 Å. Furthermore, the dynamic range of frequency shifts observed across various matrix media and the solid state for these singly halogenated complexes⁹ is much larger than that observed for CH₃CN-BF₃.⁷ On the other hand, much more muted effects were observed with larger organic substituents on the nitrile moiety, (*e.g.*, C₆H₅- or (CH₃)₃C-),⁵ because organic substituents increase the basicity of the nitrile, and in turn, stabilize the inner, bonded region of the potential curve. With shorter gas-phase B-N distances, there is less potential to contract the bond in condensed-phases.⁵

In our recent work on nitrile-BH₃ systems, we found little or no potential for medium effects, as these complexes were quite strong in the gas phase and had short B-N distances, even CF₃CN-BH₃.¹⁵ Turning to nitrile complexes of BCl₃ presents us with an opportunity to shed new light on the classic story regarding the relative Lewis acidity of BF₃ and BCl₃. Many years ago, it was noted that BCl₃ is a stronger acid than BF₃, in spite of the fact that the B-Cl bond is less polar. The long-

standing rationale for this has been that back-donation of π -electrons from the halogen to the electron deficient boron atom is more extensive for B-F bonds, as the similar size of the relevant p orbitals should lead to better overlap.¹⁶ Under this rationale, π back-bonding should also cause BF_3 to be more rigid with respect to non-planar distortion than BCl_3 .

More recently, several computational studies have led to other explanations for the greater acidity of BCl_3 , relative to that of BF_3 .¹⁷⁻¹⁹ One such study has noted that the B-X bonds in BF_3 actually have slightly less π -overlap than those in BCl_3 , which is at odds with the idea that stronger back-bonding interactions underlie the difference in Lewis acidity.¹⁷ Rather, the increased charge capacity of BCl_3 , calculated in terms of its ionization potential and electron affinity, is proposed to result in greater charge transfer, and therefore greater binding.¹⁷ Another study invokes ligand close-packing theory, which posits that geometric distortion due to the repulsive electrostatic interactions between the donor ligand and halogen substituents is the primary energetic factor.¹⁸ In turn, B-X bond distances tend to increase in order to mitigate the effect of the increased halogen-halogen repulsion caused by this distortion; as B-F bonds are stronger and more rigid than B-Cl bonds, their elongation requires more energy.¹⁸ A third study points simply to the increased covalent interactions in BCl_3 binding due to lower LUMO energy.¹⁹ In any event, this body of work deals primarily with the NH_3 ,^{17,19} and amine complexes,¹⁸ while none of them address the Lewis acidity of BF_3 or BCl_3 toward nitriles. Our recent work on BH_3 systems has noted that the differences between the structural and energetic properties of BF_3 and BH_3 complexes are much more pronounced for nitriles than they are for NH_3 .¹⁵ Furthermore, we found that the key underlying factor for this effect is that nitriles exhibit more electron-electron repulsion with the π electrons on the BX_3 moiety than does NH_3 . Because there is more π

bonding in BF_3 than BH_3 , the difference between the nitrile and amine complexes is greater for the case of BF_3 .¹⁵

Beyond the difference in structural and energetic properties between $\text{CH}_3\text{CN}-\text{BF}_3$ and $\text{CH}_3\text{CN}-\text{BCl}_3$, we are also motivated by a lack of agreement between the previous computational studies of $\text{CH}_3\text{CN}-\text{BCl}_3$.^{20,21} Two very different equilibrium structures are reported for $\text{CH}_3\text{CN}-\text{BCl}_3$ in those investigations: One with a B-N distance of 1.692 Å and a binding energy of 9.6 kcal/mol (via MP2/6-31+G(2d,p)),²¹ and another with a B-N distance of 2.793 Å and a binding energy of 6.4 kcal/mol (via MP2/TZ2P).²⁰ The former result indicates that BCl_3 may be more acidic towards nitriles than BF_3 , as the MP2/6-31+(2d,p) binding energy of $\text{CH}_3\text{CN}-\text{BF}_3$ was reported at 7.2 kcal/mol,²¹ while the latter predicts a gas-solid structure difference in which the B-N bond would contract by more than 1.0 Å upon crystallization.^{13, 20} Indeed, it was discrepancies among computational results that led us to explore the B-N bond potentials of $\text{CH}_3\text{CN}-\text{BF}_3$,⁴ which ultimately enabled us to rationalize the condensed-phase response, and illustrate that the discrepancy between the experimental and theoretical structures was genuine.⁸

In this manuscript, we report an experimental and computational study of the structural and energetic properties of $\text{CH}_3\text{CN}-\text{BCl}_3$. We studied gas-phase structural properties using both density functional theory and post-HF methods and for each model chemistry used, we found two distinct equilibrium structures separated by a significant barrier, each structure corresponding to one of the two previously reported results.^{20,21} We calculated the vibrational frequencies for each structure, and found significant differences for key structural modes. We also observed and assigned several IR bands for three isotopic forms of the complex in neon matrices, and by

comparing these data with the computed frequencies, we are able to link them to the minimum-energy structural form of the complex. In addition, we observe no signals due to the other metastable structure. Finally, we conducted an energy decomposition analysis for not only $\text{CH}_3\text{CN}-\text{BCl}_3$, but also $\text{CH}_3\text{CN}-\text{BF}_3$ and $\text{CH}_3\text{CN}-\text{BH}_3$, in an attempt to gain further insight into those factors contributing to the difference in Lewis acidity toward CH_3CN among these various BX_3 acceptors.

Experimental

Materials

Neon gas (99.999%) was obtained from Praxair and used without further purification. Acetonitrile ($\text{CH}_3\text{C}^{14}\text{N}$) was obtained from VWR and dispensed from a solvent purification system into a liquid sample tube (CHEMGLASS AF-0092). After attaching the tube to the preparatory gas manifold, the sample was degassed via several freeze-pump-thaw cycles prior to making the guest/host mixtures for the matrix experiments. CD_3CN (99.96 atom %D) and $\text{CH}_3\text{C}^{15}\text{N}$ (98 atom % ^{15}N) were obtained from Sigma-Aldrich. They were added directly to sample tubes and also degassed on the preparatory manifold prior to use. Two sources of BCl_3 were used. For the initial experiments involving $\text{CH}_3\text{C}^{14}\text{N}$, we obtained an older lecture bottle (Matheson, unknown purity) from our existing chemical inventory, and used it without further purification. For the $\text{CH}_3\text{C}^{15}\text{N}$ and CD_3CN studies, a new sample of BCl_3 was obtained from Aldrich (99.9%), and initially used without further purification. Subsequently, in order to minimize signals due to HCl and other unknown impurities in the spectra, we purified this sample by condensing about 3 mL in a liquid sample tube attached to the preparatory vacuum line, and subjected it to several freeze-pump-thaw cycles and/or brief periods of continuous evacuation at 77 K and/or 196 K.

This greatly reduced the impurity bands in the matrix spectra, but we found it impossible to completely eliminate HCl from the matrix samples.

Matrix-IR Spectra

Neon matrix spectra were obtained on a previously-described optical cryostat system.⁷ However, the pumping system has recently been replaced with a corrosive-compatible system that utilizes a turbomolecular pump (Pfeiffer TPU 261 C) with fluorocarbon oil and an inert-gas purge for the bearings. The turbomolecular pump is backed by a rotary vane mechanical pump (Pfeiffer DUO 2.5 C) that also uses a fluorocarbon-based oil. For each FTIR spectrum, 100-400 scans were averaged and the resolution was either 1 or 2 cm^{-1} . Matrices were deposited utilizing concentric dual-deposition input lines, as described previously.^{3,7} With this arrangement, separate gas mixtures were prepared for each host (*i.e.*, CH_3CN in Ne and BCl_3 in Ne) with concentrations ranging from 1/4 to 1/8 %. These samples were deposited through separate lines that merge in a concentric arrangement of two hypodermic tubes immediately prior to entering the sample chamber. Flow rates were independently controlled by Granville-Phillips #203 separate variable leak valves, and ranged from 2 to 15 mmol/hr for each mixture. The deposition temperatures ranged from 5.0 to 6.0 K. Most often, the mixtures were deposited at approximately equal rates, but in some cases, we flowed the $\text{CH}_3\text{CN}/\text{Ne}$ at a higher rate to obtain an excess of CH_3CN in the matrix. The strongest $\text{CH}_3\text{CN}-\text{BCl}_3$ peaks were observed with a composition ratio of 1/1/800 ($\text{BCl}_3/\text{CH}_3\text{CN}/\text{Ne}$) and a deposition temperature of 6.0 K. Often, samples were annealed to temperatures between 8 and 9 K to promote complex formation and in turn, aid in the identification and assignment of $\text{CH}_3\text{CN}-\text{BCl}_3$ peaks.

Computational Methods

Post Hartree-Fock, and density functional theory (DFT)²² calculations were performed using Gaussian03, vE.01,²³ and Gaussian09 vB.0.1.²⁴ Geometries were constrained to C_{3v} symmetry throughout our computational studies, though we did consider both eclipsed and staggered conformations. Convergence criteria were set using the “opt=tight” option, which sets the maximum and root-mean-square (RMS) forces to 1.5×10^{-5} and 1.0×10^{-5} hartrees/bohr, respectively, and the maximum and RMS displacements to 6.0×10^{-5} and 4.0×10^{-5} bohr, respectively. An ultrafine grid was employed for all DFT calculations.

We did explore the effects of different basis sets on the equilibrium structure results, initially with a handful of computational methods (B3LYP, B3PW91, and MP2),²² and the 6-311G(d) and 6-311+G(d) basis sets, with an eye towards the effect of diffuse functions.⁴ However, we found that the effects of including (or excluding) diffuse functions in the basis set were minimal. Ultimately, we employed a variety of DFT methods and MP2 with the aug-cc-pVTZ basis set, as well as a variety of post-HF methods with the 6-311+G(2df,p) basis set. For equilibrium structures, we chose to report both MP2/aug-cc-pVTZ as well as select *mPW1* /aug-cc-pVTZ results. Our rationale was as follows: In order to identify an acceptable method for frequency predictions, we conducted a validation study to determine which method among MP2 and 19 different pure and hybrid density functional methods (B1B95, B3LYP, B3PW91, B97-2, B98, BH&HLYP, BLYP, BMK, BPW91, HCTH, HSEh1PBE, M06, M06-2X, *mPW1*, O3LYP, OLYP, TPSSh, ω B97, and X3LYP) would best reproduce experimental frequencies of free BCl_3 . Of these, we found that five methods had RMS errors of less than 10 cm^{-1} : B1B95 (8.0 cm^{-1}), B3PW91 (7.9 cm^{-1}), B97-2 (7.5 cm^{-1}), HSEh1PBE (7.6 cm^{-1}), and *mPW1* (7.5 cm^{-1}). Of these, we chose to use *mPW1*

and B3PW91 to make structure and frequency predictions for the CH₃CN–BCl₃ complex, mainly for the sake of consistency with prior work; these two methods were among also the best performers in an analogous validation studies involving nitrile-BF₃ systems.^{6,25} In the present case, however, we were left without a gas-phase structure against which to validate the equilibrium structural results. So, we took the approach that we did with our studies of nitrile BH₃ complexes,¹⁵ and report the MP2/aug-cc-pVTZ results in the figure below, together with DFT results (*mPW1* in this case) for structural parameters that are significantly different between methods. The slight preference for the *mPW1* structure (and frequency) results over those from B3PW91 stems from a slightly better agreement with MP2 for the structural properties. We also note that we did apply an empirical scale factor (of 0.9525) for comparisons involving calculated CN-stretching frequencies, for which the predictions are marginal. This was determined directly from the ratio of observed (neon matrix) ν_{CN} values from CD₃CN (which lacks the Fermi resonance doubling that occurs in CH₃CN).²⁶

The B-N potential was mapped in a point-wise manner by computing the energies at a series of fixed B-N distances ranging from 1.3 to 3.5 Å in 0.1 Å steps, with additional points at 3.7 and 3.9 Å. DFT methods used to map the potential included B3PW91, and *mPW1* (those used for the structure and frequency predictions), and well as B97-2 (which performed best for the CH₃CN–BF₃ potential),⁸ all with the aug-cc-pVTZ basis set. The exception was that we did also compute a B97-2/aug-cc-pVQZ curve to assess the effect of basis set size and the extent of convergence. There was no chemically-significant difference between these curves; the overall shape was the same, but the B97-2/aug-cc-pVQZ points were simply 0.2 to 0.3 kcal/mol higher in energy across most of the curve. Also, for the DFT curves, all degrees of freedom beyond the B-N distance were

optimized at every point. Post-HF methods used to map the potential included MP2, MP3, MP4 (DQ), and CCSD. For all methods beyond MP2, we used the 6-311+G(2df,p) basis set, though we computed an MP2/aug-cc-pVTZ curve for direct comparison to the DFT results. We also note that for levels beyond MP2, the geometries were not optimized at each level of theory; the points displayed below are the post-HF energies at the MP2/6-311+G(2df,p) geometries. The effects of bulk dielectric media, were explored using the PCM model and the B97-2 functional (PCM/B97-2/aug-cc-pVTZ), with ϵ values ranging from 1.2 to 24.0. As in our past work,⁸ we constructed hybrid potential curves by adding the electrostatic component of the solvation free energy to the gas-phase electronic energy at each point on the curve.

Energy decomposition analyses (EDA), using the method of Morokuma,²⁷ were carried out using the Amsterdam Density Functional (ADF) Program, version 2008.01.²⁸ For these calculations, the TZ2P basis set²² was used for all hydrogen atoms and the ATZ2P²² basis set for all heavy atoms. No use of the frozen core approximation was made. The equilibrium geometry for the donor-acceptor complex was optimized with the generalized gradient approximation (GGA) *mPW* functional²² until the maximum matrix element of Cartesian gradients was reduced to 1.0×10^{-7} hartree/angstrom. A decomposed mapping of the donor-acceptor bond potential was obtained by conducting an EDA analysis with the donor-acceptor distance frozen at every 0.1 Å interval between 1.0 Å and 3.2 Å, and at every 0.2 Å interval between 3.2 Å and 4.0 Å. All other degrees of freedom were optimized in this process with a method analogous to the one used for the equilibrium geometry, except that the convergence criterion was loosened to a value of 5.0×10^{-5} hartree/angstrom. All EDA analyses were carried out using single point calculations with the *mPW1*²² hybrid GGA functional at the *mPW* optimized geometries described above.

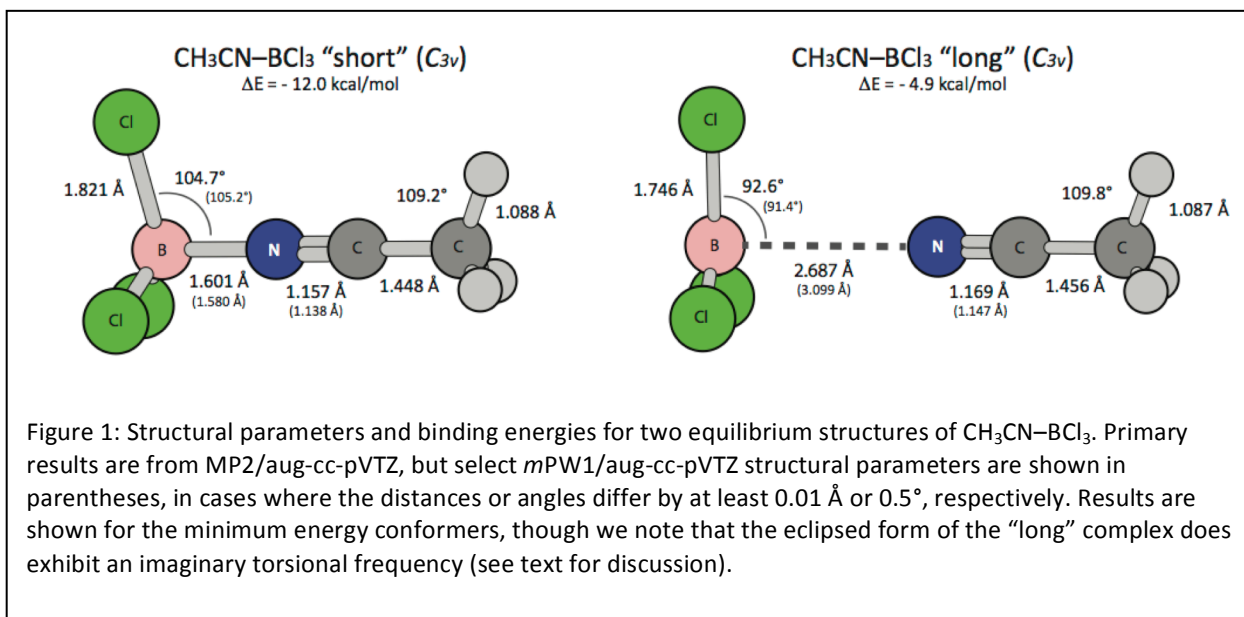
Results and Discussion

Equilibrium Structures

The first goal of our computational investigation was to identify the minimum-energy, equilibrium structure of $\text{CH}_3\text{CN}-\text{BCl}_3$. Above, we noted that the first predicted structure in the literature, obtained via MP2/TZ2P, had a B-N distance of 2.793 Å,²⁰ while the more recently published result (via MP2/6-31+G(2d,p)) had a B-N distance of 1.692 Å.²¹ We had initially presumed, based on prior experience with $\text{CH}_3\text{CN}-\text{BF}_3$,⁴ that the discrepancy resulted from the inclusion or exclusion of diffuse functions (signified by “+”) in these basis sets. However, in our preliminary assessments using a few DFT methods and MP2 with the 6-311G(d) and 6-311+G(d) basis sets, we found that we could obtain structures similar to either of the previously-published results, and that the key, determining factor was the initial B-N distance, not the basis set (nor the method). That is, optimizations started from short B-N distances (1.5-1.7 Å) provided structures with B-N bonds of about 1.6 Å, and those initiated at long (2.5-3.0 Å) B-N distances delivered structures with final distances near 3.0 Å, even with tight convergence criteria.

As we moved to higher-level examinations of the equilibrium structural properties, we used the methods noted above (B3PW91, *mPW1* , and MP2) with the aug-cc-pVTZ basis set, and furthermore, we performed two distinct optimizations for each method with starting B-N distances of 1.5 Å and 3.0 Å. The structure results among the DFT methods were very consistent: the B-N distances obtained with B3PW91 and *mPW1* were 1.581 Å and 1.580 Å for the “short-bond” structure, and 3.237 Å and 3.099 Å for the “long-bond” structure, respectively. The MP2 results for the short structure were reasonably consistent with the DFT results, with a B-N

distance just slightly longer (1.601 Å). For the long-bond structure, the MP2 (2.687 Å) distance was notably shorter than those computed from DFT, presumably because MP2 provides a better accounting of dispersion than the older-generation density functionals, and such interactions may comprise a significant part of the interaction energy for the long-bond complex.



The MP2/aug-cc-pVTZ binding energies for these “short” and “long” structures were 12.0 and 4.9 kcal/mol, respectively, and indicate that the short structure is the global minimum and lies about 7.1 kcal/mol lower in energy. Our previous results for $\text{HCN}-\text{BF}_3$ ²⁵ would suggest that these binding energies slightly overestimate true values. However, we note that those from higher-level post-HF methods (albeit with a slightly smaller basis set) can be inferred from the B-N potential curves displayed below, and indeed, they are slightly smaller in magnitude than the MP2 value. Complete sets of parameters for both equilibrium structures, in the eclipsed conformation, are displayed in Figure 1. We chose to emphasize the MP2 results in the figure, though this preference is somewhat arbitrary, and because the frequency predictions are based on the *mPW1*

structures, the values of those parameters are included in parentheses in cases where the distances and angles, that differ by more than 0.01 Å or 0.5°, respectively.

Throughout this work, we focus mainly on the eclipsed conformation, in part because it was found to be the minimum energy isomer by Cheong and Cho (albeit for a short-bond-like structure),²¹ and moreover, they examined this issue in depth. When we obtained frequencies for the short-bond structures, we found the values for the torsional mode to be real, and reasonably large given the nature of this motion (32 cm⁻¹ for *mPW1/aug-cc-pVTZ* and 31 cm⁻¹ for *B3PW91/aug-cc-pVTZ*). Also, these were consistent with the values reported by Cheong and Cho (28 cm⁻¹), who also reported a rotation barrier of about 47 cal/mol.²¹ However, when we turned our attention to the long-bond structure, we obtained results that were inconclusive with regard to the equilibrium conformation, but they did indicate, above all else, that there is essentially free rotation in the torsional degree of freedom. We first noted that the *mPW1* and *B3PW91* torsional frequencies for the eclipsed, long-bond structure were imaginary (9i cm⁻¹ for both methods). However, for the staggered conformation we obtained an imaginary torsional frequency with *mPW1* (4i cm⁻¹), and a small, real value via *B3PW91* (1 cm⁻¹). We did find that the eclipsed form was lower in energy, though only by 2.9 cal/mol (*MP2/aug-cc-pVTZ*). Thus, for the sake of consistency having focused on the eclipsed conformer in mapping the B-N bond potential (see below), and because it is clearly the more stable form at short B-N distances, we choose to report structural parameters for the eclipsed form of the long-bond structure in Figure 1. However, there are no chemically-significant differences in the parameters between the two conformers.

The differences between the long-bond and short-bond structures are extreme. The former is indicative of a very weak, non-bonded complex, and the binding energy (4.9 kcal/mol)

corroborates that characterization. As such, the B-N distance of 2.7 to 3.0 Å is only somewhat shorter than the sum of the B and N van der Waals radii (3.47 Å).²⁹ The short-bond structure, on the other hand, is consistent with a strong donor-acceptor interaction. The B-N distance is about 1.6 Å, comparable to the sum of the covalent radii (1.55 Å).³⁰ In fact, this is significantly shorter than the calculated B-N distances for H₃N-BCl₃ (1.62 Å),¹⁷⁻²⁰ in spite of the fact that the binding energy is much lower (the MP2/aug-cc-pVTZ value for H₃N-BCl₃ is 23.1 kcal/mol).¹⁹ This situation mimics our experience with borane complexes,¹⁵ and as such, it presumably reflects the differences in hybridization of the N-donor atom, and to some extent, the greater extent of electron-electron repulsion between the nitrile donor and the BCl₃ moiety (see below). Since amines have a more extended, sp³-like donor orbital, they can achieve significant overlap at longer B-N distance than nitriles, which utilize a less-extended, sp-like donor orbital. Also, because the nitriles must approach more closely for significant overlap, there is greater electron-electron repulsion, and a lower binding energy than with amines.¹⁵

B-N Bond Potentials

B-N bond potentials obtained from both DFT and post Hartree-Fock calculations are displayed in Figure 2. Above all else, they all exhibit two distinct minima along the B-N coordinate. Furthermore, these minima are separated by a significant barrier. According to DFT (B3PW91, *m*PW1, or B97-2, with the aug-cc-pVTZ basis set), the global short-bond minimum near 1.6 Å lies about 5-8 kcal/mol below the energy of the separated fragments. On the other hand, the long-bond minimum occurs near 3.2 Å, and lies only 0.8 to 1.4 kcal/mol below free CH₃CN and BCl₃, and the barrier between the minima lies 1.4 to 2.8 kcal/mol above the outer, secondary minimum. The post-HF results indicate that the global minimum lies at a somewhat lower energy, and for levels of theory beyond MP2, that the barrier is also slightly larger. With MP2/aug-cc-pVTZ, the

inner, global minimum lies near -12 kcal/mol but is about 1 kcal/mol higher in energy with the 6-311+G(2df,p) basis set. Also, longer, secondary minima occur at notably shorter distances than with DFT (2.7 to 2.8 Å), and lie at somewhat lower energies (4.5 to 5.0 kcal/mol). Also, the barrier is rather slight, rising only 0.3 kcal/mol above the outer, secondary minimum with aug-cc-pVTZ, and only 0.6 kcal/mol with the 6-311+G(2df,p) basis set. The energies along the B-N coordinate are much more consistent among post-HF methods beyond MP2 (CCSD, MP4(DQ), MP4(D), and MP3 with the 6-311+G(2df,p) basis set, of which the latter two were excluded from the figure for clarity. The inner global minima lie between -7.7 and -8.6 kcal/mol, and the outer, secondary minima occur at about 2.9 Å with energies of -3.4 to -3.6 kcal/mol, relative to free BCl₃ and CH₃CN. Also, the barriers lie between 1.6 and 2.4 kcal/mol above the outer minima. We did also calculate a few CCSD(T)/6-311+G(2df,p) energies at select points to further verify the occurrence of the distinct minima. The CCSD(T) energies at 1.6, 2.2, and 2.9 Å were -8.5, -2.5, and -4.0 kcal/mol, respectively, and are reasonably consistent with other post-HF results beyond MP2. Relative to CCSD/6-311+G(2df,p), both minima lie a few tenths of a kcal/mol lower in energy, and that the barrier is slightly less (1.5 kcal/mol above the outer minimum). Regardless, the two distinct minima and the barrier persist are highest levels of theory that we were able to access.

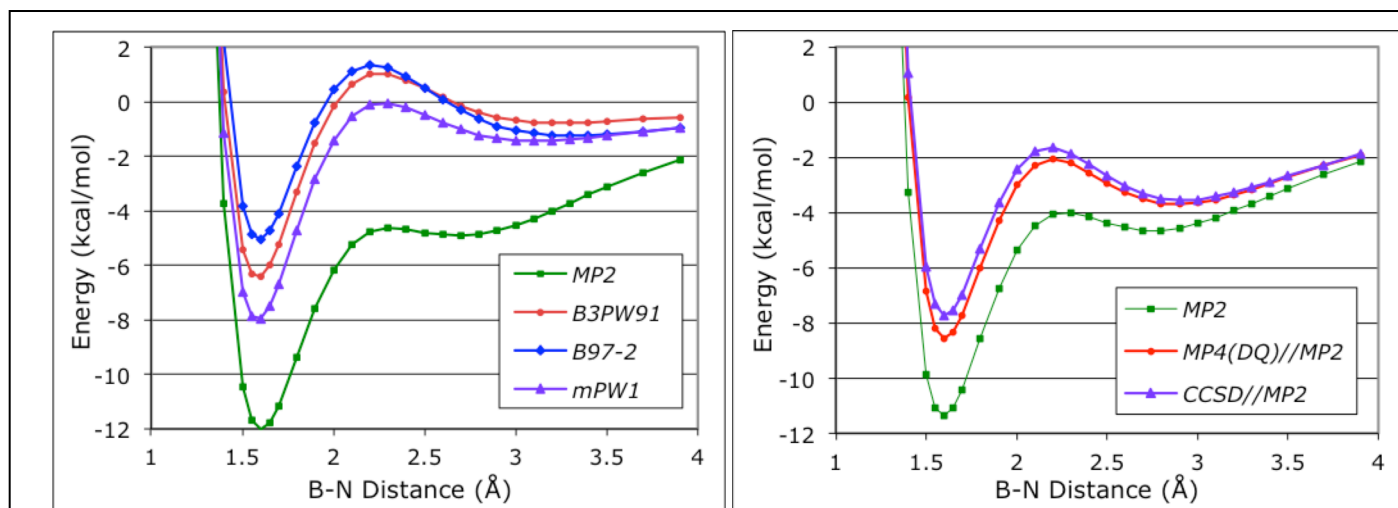


Figure 2: Calculated B-N bond potentials for $\text{CH}_3\text{CN}-\text{BCl}_3$ using a few hybrid DFT methods (and MP2) with the aug-cc-pVTZ basis set (left) and various post-HF methods with the 6-311+(2df,p) basis set (right). MP2 data is included in each graph for reference purposes, though we note that the energies are about 1 kcal/mol higher across most of the curve with the 6-311+G(2df,p) basis set (right). The MP4(DQ) and CCSD energies on the right-hand graph are based on the MP2/6-311+(2df,p) geometries.

To assess how bulk, condensed-phase media may affect the relative stability of the minima on the B-N potential, and/or the barrier between these minima, we also mapped the potential in the presence of dielectric media using the PCM model in a manner we had done previously for $\text{CH}_3\text{CN}-\text{BF}_3$.⁸ In this approach, we took the electrostatic component of the Gibbs energy of solvation, and added that to the gas-phase electronic energy, producing a hybrid energy surface that represents the bond potential in the bulk dielectric medium. A set of curves generated using PCM/B97-2/aug-cc-pVTZ, is displayed in Figure 3. We chose the B97-2 functional for two reasons, one being consistency with past work, as it was effective for predicting medium effects on structure of $\text{CH}_3\text{CN}-\text{BF}_3$.⁸ Furthermore, B97-2/aug-cc-pVTZ is the DFT method which most closely reproduced the CCSD/6-311+G(2df,d) energy difference between the global minimum and the barrier. In any event, as in other systems, the addition of the solvation free energy provides

more stabilization to the inner portion of the curve. The reason for this is a larger dipole at shorter B-N distances, resulting from more charge transfer from donor to acceptor, as well as more distortion in the BX_3 subunit.⁸ In contrast to analogous nitrile- BF_3 systems,⁸ the effect of the medium on the potential is only a slight lowering along the inner wall near the minimum. However, the preferential stabilization towards shorter B-N distances does essentially double the barrier height relative to the global minimum (from 6.4 to 13.4 kcal/mol). In any event, these curves indicate that bulk, condensed-phase media cause only subtle changes in the structural properties of $CH_3CN-BCl_3$. Thus, we would not expect that medium effects would obscure, to any great extent, comparisons between calculated gas-phase frequencies and experimental data from neon matrices.

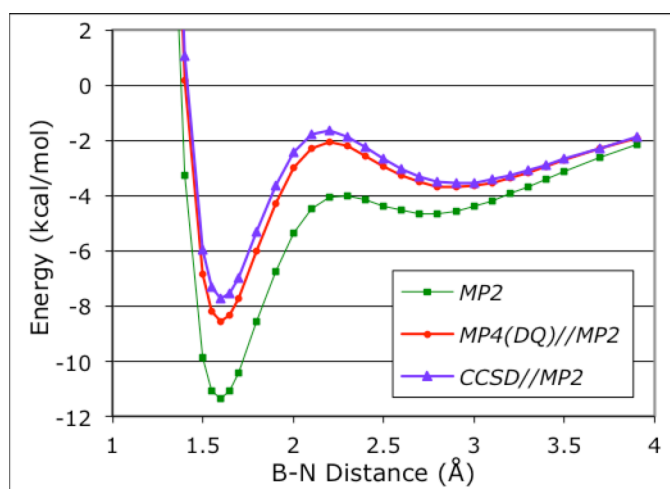
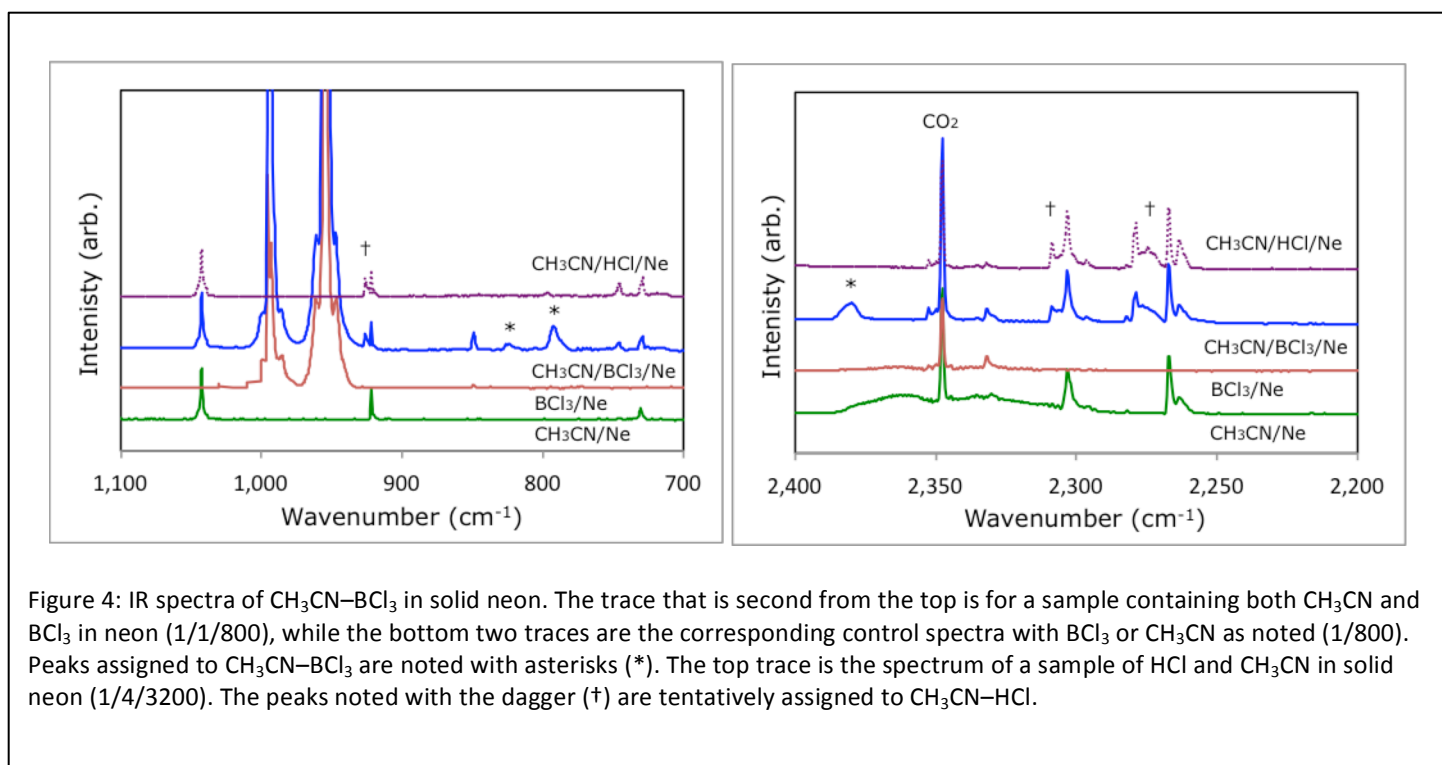


Figure 3: Calculated B-N bond potentials for $CH_3CN-BCl_3$ in bulk, dielectric media (PCM/B-97-2/aug-cc-pVTZ), with ϵ -values ranging from 1.0 (gas-phase) to 24.0. The curves for $\epsilon > 1$ are hybrid potentials in which the electrostatic component of the solvation free energy is added to the gas-phase electronic energy, as in ref 8.

Infrared Spectra & Frequencies

We collected a series of IR spectra for neon matrices containing BCl_3 and one of three isotopic forms of CH_3CN and, ultimately, we made definitive assignments of three key bands for each of six isotopic forms of $\text{CH}_3\text{CN-BCl}_3$. The spectra are displayed in Figures 4 – 6, and frequencies are listed in Table 1, together with calculated $m\text{PW1/aug-cc-vPTZ}$ predictions for the assigned bands, as well as those measured previously for the solid complex.³¹ A complete listing of $m\text{PW1/aug-cc-vPTZ}$ and $\text{B3PW91/aug-cc-pVTZ}$ frequencies for the primary isotopomers of both long-bond and short-bond forms of the complex is included as supplementary information (Tables S1 & S2, respectively). We note here that the $m\text{PW1}$ and B3PW91 results are reasonably consistent with each other, and with the MP2/6-31+G(2d,p) results in reference 21 for the short-bond complex.

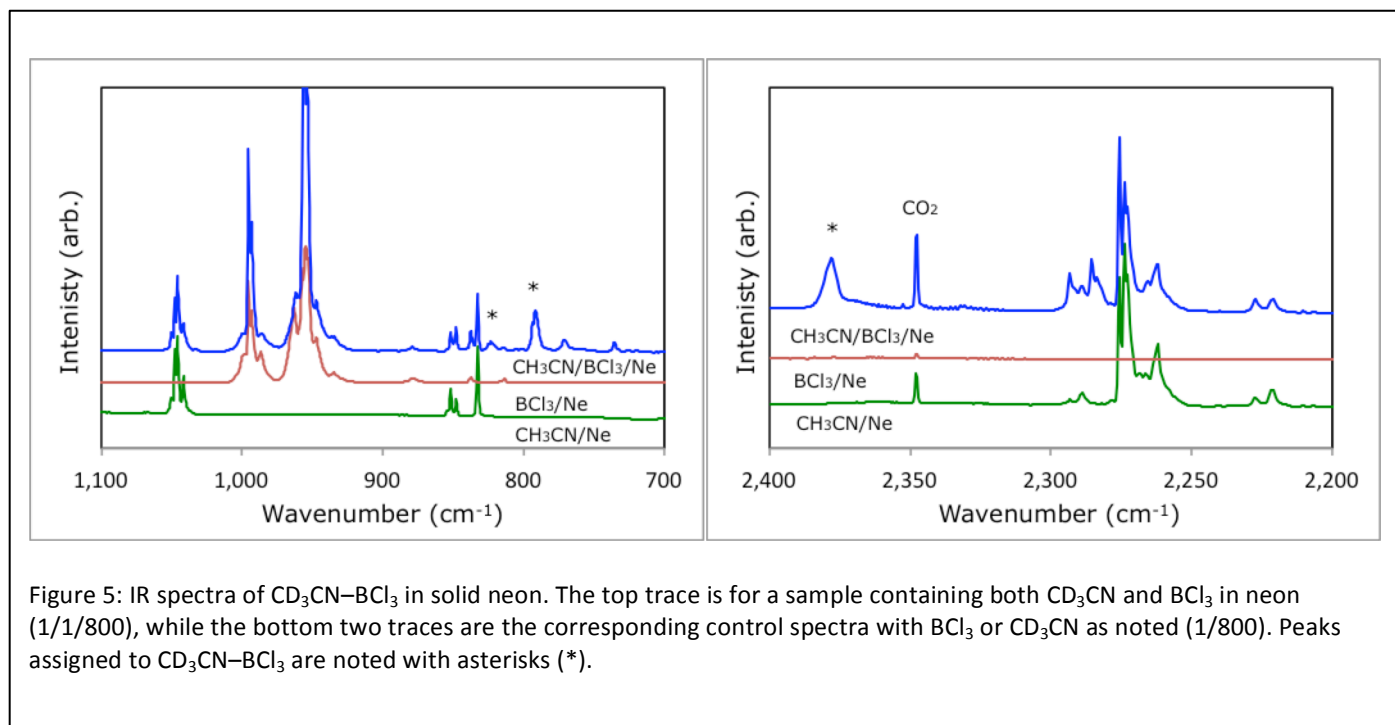


Turning first to the spectra for the non-enriched CH₃CN samples (Figure 4), we observed a prominent set of product bands, i.e., peaks that required both BCl₃ and CH₃CN, at 792, 824, and 2380 cm⁻¹, together with a series of minor product bands at: 618/622 (a doublet), 926, 2308, and 2280 cm⁻¹. Some weaker features were observed in some experiments as well, these occurred at 636, 642, and 746 cm⁻¹, as well as an overlapped group ranging from 654 to 666 cm⁻¹ that appears mainly upon annealing. The pair at 792 and 824 cm⁻¹ exhibited the characteristic 4:1 intensity ratio expected for a ¹¹B/¹⁰B isotopic pair, as well as splitting (32 cm⁻¹) that agreed well with the isotope splitting we observe for the B-Cl asymmetric stretching mode in un-complexed BCl₃ (39 cm⁻¹).³² We also note that the calculated (*m*PW1/aug-cc-pVTZ) isotope shift for this band in the short-bond form of the CH₃CN–BCl₃ complex is 33 cm⁻¹, and the frequency predictions themselves lie within 10 cm⁻¹ of the observed peaks. Thus, we assign the peaks at 792 and 824 cm⁻¹ to the B-Cl asymmetric stretching (ν_{BCl}^a) bands of CH₃CN–¹¹BCl₃ and CH₃CN–¹⁰BCl₃, respectively. We subsequently noted that the band at 2380 cm⁻¹ exhibited consistent relative intensities with the ν_{BCl}^a bands across all conditions studied, and given that this frequency lies in the CN stretching region and is coincident with the value of the ν_{CN} band observed for the solid complex,³¹ we so assign it (the ¹⁵N isotope shift will be discussed below). We note that the ¹⁰B/¹¹B isotope shift predicted for this band is less than 1 cm⁻¹. One of the weaker product bands, a doublet (618/622) centered at 620 cm⁻¹, was also found to exhibit consistent intensities relative to the ν_{BCl}^a bands, and the only reasonable candidate for an assignment would be the BCl₃ symmetric bending or “umbrella” mode (δ_{BCl}^s). The *m*PW1 prediction for the δ_{BCl}^s band of the short-bond form of the complex is 667 cm⁻¹, and for the solid a peak originally assigned to the ¹¹B-N stretching mode is observed at 719 cm⁻¹ (the ¹⁰B counterpart is seen at 742 cm⁻¹).^{21, 31}

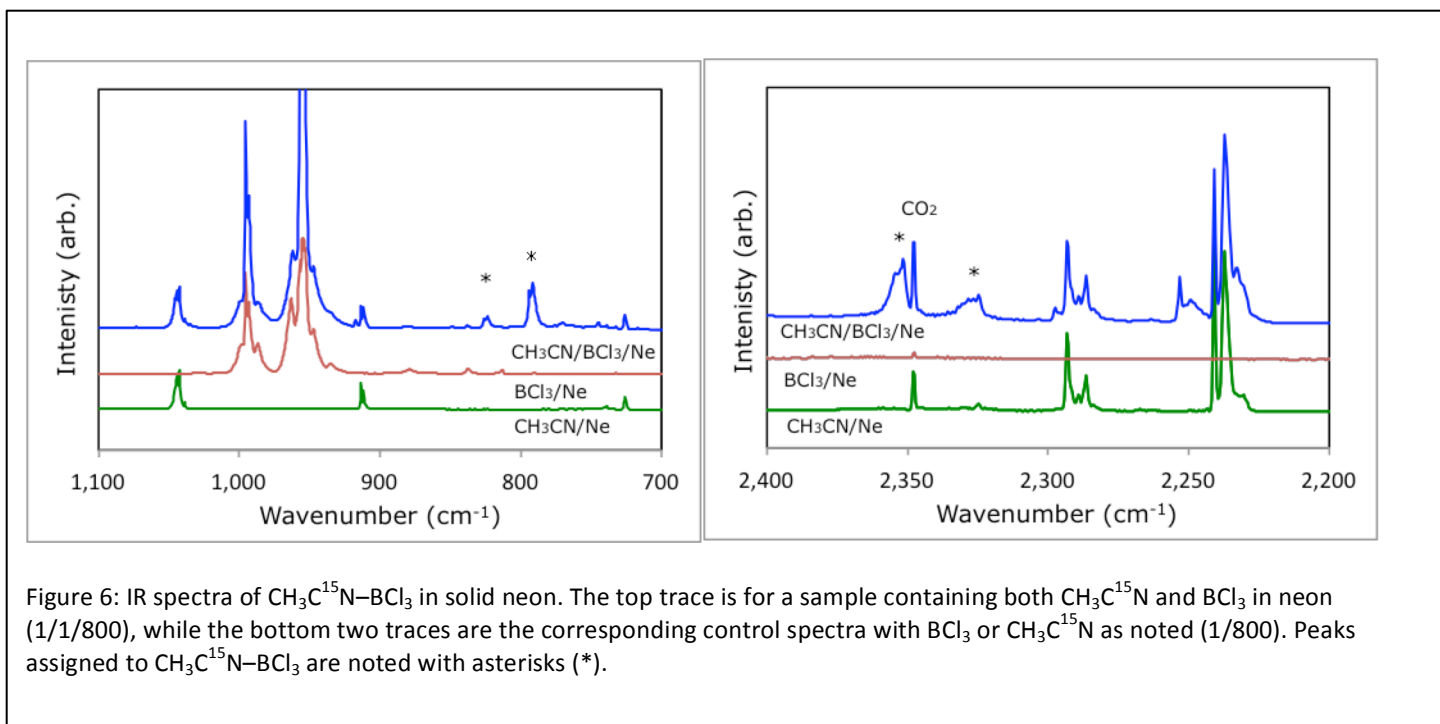
Previously, Cheong and Cho predicted a value of 648 cm^{-1} (via MP2/6-31+G(2d,p)) and furthermore, a coupling analysis indicated that this frequency corresponded to a mix of three a_1 -symmetry modes including the BCl_3 symmetric deformation (40%), the B-N stretch (25%), and the BCl_3 , symmetric stretch (29%).²¹ Nonetheless, their predicted $^{11}\text{B}/^{10}\text{B}$ isotope shift for this band is identical to our *mPW1* prediction (27 cm^{-1}), and this is a region for which we observe several weak absorption features. One of these, at 642 cm^{-1} , has an intensity that is approximately $\frac{1}{4}$ that of the 620 cm^{-1} band, and this would agree marginally well with the predicted isotope shift. Nonetheless, the agreement between the spectrum of the solid complex and the predictions is marginal, and may result from the coupling of the three low-frequency, a_1 -symmetry modes that occur within the BCl_3 subunit complex, with that coupling sensitive to subtle structural changes and/or medium effects. This, and the absence of a definitive isotope shift, makes it difficult to assign the 620 cm^{-1} peak and its potential counterpart at 642 cm^{-1} to a particular vibrational mode.

We also noted a consistent set of intensity ratios among the other weak product bands, at 926 cm^{-1} , 2308 cm^{-1} , and the doublet consisting of one sharp (2279 cm^{-1}) and one broader (2275 cm^{-1}) peak. The last two peaks lie just to the blue of the components of the Fermi resonance doublet for the ν_{CN} band in un-complexed CH_3CN .³³ However, these were distinct from those of the peak assignments discussed immediately above. Moreover, since they agree rather favorably with the *mPW1* predictions for the long-bond form of the complex, we initially suspected that both structural forms of the complex may be present in the neon matrix. However, we also noted a prominent product feature near 2677 cm^{-1} , which lies just below a series of bands between about 2750 and 2900 that have been previously assigned to HCl and HCl clusters.³⁴ This latter

observation indicates a significant amount of HCl impurity in the samples, which persisted after several refinements to the sample preparation and depositions processes. While the IR spectrum of $\text{CH}_3\text{CN-HCl}$ has been measured in both argon and nitrogen matrices,³⁵ it has not yet been studied in neon, so we subsequently conducted some experiments with HCl and CH_3CN , and we confirmed that this group of weaker bands with consistent peak areas was $\text{CH}_3\text{CN-HCl}$, and not the long-bond form of the $\text{CH}_3\text{CN-BCl}_3$ complex. We include a trace in Figure 4 for the spectrum of an HCl- and CH_3CN -containing sample to illustrate this, and we are now in the process of a more thorough study of the $\text{CH}_3\text{CN-HCl}$ complex; thus we defer any further discussion of these frequencies to a future manuscript. We have no assignments for the other weak product bands observed in this region.



We observed analogous sets of product bands in the IR spectra of the neon matrices containing BCl_3 and isotope-enriched forms of CH_3CN (CD_3CN and $\text{CH}_3\text{C}^{15}\text{N}$). In the $\text{CD}_3\text{CN}/\text{BCl}_3$ experiments, strong product bands were observed at 792, 823, and 2378 cm^{-1} . Also, a series of weaker bands was observed at 616 (as a doublet 615/617), 630, 642, 837, 735, 814, 2285/2283 cm^{-1} (a broad multiplet), as well an overlapped group ranging from about 646-670 cm^{-1} (often only upon annealing). The pair at 792 and 823 was assigned to the ν_{BCl}^a bands of $\text{CD}_3\text{CN}-^{11}\text{BCl}_3$ and $\text{CD}_3\text{CN}-^{10}\text{BCl}_3$, respectively, on the basis of the characteristic 4/1 intensity ratio, and the $^{10}\text{B}/^{11}\text{B}$ isotope splitting (31 cm^{-1}) which was consistent with the predicted $^{11}\text{B}/^{10}\text{B}$ shift (33 cm^{-1}). The other prominent band (2378 cm^{-1}) was assigned to the ν_{CN} band on the basis of intensity ratios. Also, we found that the band at 616 cm^{-1} exhibited consistent intensity ratios with the major product bands noted above. This band seems analogous to the 620 cm^{-1} band observed in the CH_3CN -containing spectra (*i.e.*, referred to tentatively as δ_{BCl}^s band, though the mode is coupled with two other a_1 -symmetry motions), and once again we observe a possible candidate for the ^{10}B counterpart at 642 cm^{-1} . Again, we found it difficult to make a definitive assignment for this band. The remaining weaker bands, at 837 and 2283/85 cm^{-1} exhibit consistent intensity ratios with a prominent product feature at 2677 cm^{-1} , and thus we presume this set of peaks, which are entirely analogous to those noted above in the analysis of the non-enriched CH_3CN sample, arise from $\text{CD}_3\text{CN}-\text{HCl}$. We have no assignments for the other weak product bands observed in these spectra.



In the $\text{CH}_3\text{C}^{15}\text{N}/\text{BCl}_3$ experiments, we observed IR bands that were very much analogous to those in the experiments involving other CH_3CN isotopomers. These included a prominent set of product bands at 793, 825, 2328, and 2353 cm^{-1} , in addition to a weaker series at 620 (as a doublet at 618/622), 636, 648, 2296 and 2249/2253 cm^{-1} (a broad multiplet) and again, a very weak, overlapped set of bands ranging from about 655-680 cm^{-1} that is most readily observed upon annealing. Once again, we assigned the pair at 793 and 825 cm^{-1} to the ^{11}B and ^{10}B components of the ν_{BCl}^a band of $\text{CH}_3\text{C}^{15}\text{N}-\text{BCl}_3$, respectively, on the basis of the characteristic 4/1 intensity ratio and the agreement between the observed (32 cm^{-1}) and predicted isotope splitting (33 cm^{-1} , short-bond structure). The pair of bands at 2328 and 2353 cm^{-1} also exhibit consistent intensity ratios with the ν_{BCl}^a bands, and we presume that they correspond to the CN-stretching bands, and the Fermi resonance between the ν_{CN} and $\nu_3 + \nu_4$ bands³³ persists in the matrix isolated complex. We note that

for the solid complex³¹ there were bands observed at 2360 and 2329 cm⁻¹, though they only identified the 2329 cm⁻¹ band with the ν_{CN} mode. We predict a ¹⁵N/¹⁴N isotope shift of 32 cm⁻¹ for this band (*mPW1/aug-cc-pVTZ*, scaled, short-bond structure), and thus we'd expect the peak at 2348 cm⁻¹, in reasonable agreement with the 2353 cm⁻¹ band, and this lends some confidence to all the ν_{CN} band assignments. The additional peak does complicate the issue of an isotope shift, however. Once again, we also noted that the weaker product bands at 620 cm⁻¹, exhibited consistent intensity ratios with the major, assigned product bands, and also, there is a possible ¹⁰B counterpart at 648 cm⁻¹. But once again, poor agreement with the solid data and predictions, and well as a marginal peak area measurement for the weaker component do not permit a definitive assignment. In addition, we note that the group of peaks at 917, 2296, and 2251 cm⁻¹ appear to be analogs of the bands we assigned to the CH₃CN–HCl complex in the experiments with the primary isotopomer of CH₃CN.

Table 1: Measured and calculated frequencies for CH₃CN–BCl₃.¹

Isotopomer\Mode	BCl ₃ Asymmetric Stretch			C-N Stretch		
	<i>neon</i> ²	<i>calc</i> ³	<i>solid</i> ⁴	<i>neon</i> ²	<i>calc</i> ^{3,5}	<i>solid</i> ⁴
CH ₃ CN– ¹¹ BCl ₃	792	782	746	2380	2362	2380
CH ₃ CN– ¹⁰ BCl ₃	824	815	777		2362	2381
CD ₃ CN– ¹¹ BCl ₃	792	782	750	2378	2361	2371
CD ₃ CN– ¹⁰ BCl ₃	823	815	774		2362	2372
CH ₃ C ¹⁵ N– ¹¹ BCl ₃	793	782	-	2328/2353	2329	-
CH ₃ C ¹⁵ N– ¹⁰ BCl ₃	825	815	775		2329	2329/2360

1) Units of cm⁻¹. 2) This work. Experimental uncertainty, based on peak reproducibility is ± 1 cm⁻¹. 3) *mPW1/aug-cc-pVTZ* prediction for a structure with R(B-N) = 1.580 Å. 4) Ref. 31. 5) Values for the C-N stretching band were scaled by factor of 0.9525, determined from the ratio of the observed to calculated ν_{CN} frequencies for CD₃CN. See text for discussion.

The frequencies of the assigned peaks in the neon matrix spectra, as well as observed isotope splittings, clearly indicate that we are observing a complex with structure with a short B-N bond near 1.6 Å. For the BCl₃ asymmetric stretching bands, the observed peaks lie within 11 cm⁻¹ of the *mPW1* predictions for the short bond structure (R(B-N) = 1.580 Å). The frequencies for these modes in the solid complex, however, are red-shifted 40-50 cm⁻¹ from those in the neon matrix. A possible explanation for this is that intermolecular interactions in the solid cause a slight contraction of the B-N bond relative to the structure in the gas-phase and/or neon matrix, and we note that the potential does show very slight signs of softening along the inner wall in dielectric media (above). Also, the BCl₃ stretching mode does shift systematically to lower frequencies as the bond contracts. This is illustrated by the difference in the predicted (*mPW1/aug-cc-pVTZ*) frequencies of this mode for both structural forms of the CH₃CN-¹¹BF₃ complex, 782 cm⁻¹ for R(B-N) = 1.580 Å and 957 cm⁻¹ for R(B-N) = 3.099 Å. We also note that we explicitly explored the variation of the B-N distance dependence of the analogous mode for CH₃CN-BF₃ and noted a monotonic shift to lower frequencies with decreasing R(B-N).⁴ Thus, the difference in bands between the solid and matrix data could reflect a slight structural difference, as the B-N distance in the crystal is 1.562(8) Å and the MP2/*aug-cc-pVTZ* prediction is 1.601 Å. We also note that the *mPW1* frequencies are based on a structure with slightly shorter distance than the MP2 value of 1.58 Å, and that the predictions are 9-11 cm⁻¹ red shifted from the matrix values. In any event, the isotope shift shifts for the ν_{BCl}^a band (33 cm⁻¹) in the short-bond form of the complex also compare much more favorably to the observations (31-32 cm⁻¹) than those for the long bond form (40 cm⁻¹). There is also a great deal of consistency between the matrix and solid-state values of the C-N stretching frequencies,³¹ and a reasonable agreement between these and the predictions for the short-bond form of the complex. In both the CH₃CN and CD₃CN spectra, we observe the CN bands very near those of the solid. The frequency predicted for the short-bond form of

$\text{CH}_3\text{CN}-^{11}\text{BCl}_3$ is 2361 cm^{-1} (scaled), while that predicted for the long-bond form is 2283 cm^{-1} (scaled). Thus, it is clear that the structure of the complex that we are observing in the matrix resembles that of that of the short-bond structure and/or the solid, and not the long-bond structure that corresponds to the secondary minimum on the B-N potential. We do note that our experimental conditions would make the observation of the long-bond form of $\text{CH}_3\text{CN}-\text{BCl}_3$ rather difficult, should it be present to some extent in the matrix sample. The predictions for the stronger CH_3CN -localized modes of the long-bond form of $\text{CH}_3\text{CN}-\text{BCl}_3$ are near the peaks we have observed and assigned to $\text{CH}_3\text{CN}-\text{HCl}$. As for the BCl_3 -localized modes, most occur at relatively low frequencies where we have marginal signal-to-noise ratios in the spectra, and the exception, the ν_{BCl}^a bands, are shifted so slightly that they would be obscured by the broad, strong ν_{BCl}^a bands of un-complexed BCl_3 .

Energy Decomposition Analyses

In order to identify the reasons for the substantial differences in the structural and energetic properties of $\text{CH}_3\text{CN}-\text{BCl}_3$ and two analogous complexes, $\text{CH}_3\text{CN}-\text{BH}_3$ and $\text{CH}_3\text{CN}-\text{BF}_3$, we conducted energy decomposition analyses (EDA) on these systems. Previous MP2/aug-cc-pVTZ calculations,¹⁵ have predicted $\text{CH}_3\text{CN}-\text{BH}_3$ to be a strong complex ($\Delta E = -22.6\text{ kcal/mol}$), with a short (1.58 \AA) B-N distance, and $\text{CH}_3\text{CN}-\text{BF}_3$ to be a fairly weak complex ($\Delta E = -8.7\text{ kcal/mol}$), with a relatively long *equilibrium*⁸ B-N distance (1.82 \AA). The properties of $\text{CH}_3\text{CN}-\text{BCl}_3$, as described above, are intermediate to some extent; the B-N distance (for the global minimum structure) is short and comparable to that of $\text{CH}_3\text{CN}-\text{BH}_3$, but the binding energy is small and comparable to $\text{CH}_3\text{CN}-\text{BF}_3$. We also note substantial differences in the topological features of the B-N potential energy surfaces. The potential for $\text{CH}_3\text{CN}-\text{BF}_3$ is broad and flat, and the energy rises by only about 0.5 kcal/mol between 1.8 \AA , the equilibrium distance, and 2.5 \AA .⁸ The potential energy surface for $\text{HCN}-\text{BH}_3$, on the other

hand, exhibits a reasonably deep well, localized in the region of the equilibrium bond distance. Neither potential energy surface exhibits two distinct minima as does that of $\text{CH}_3\text{CN}-\text{BCl}_3$.

In the EDA scheme, the binding energies (ΔE) are partitioned according to the scheme outlined in equation (1).^{36,37}

$$\Delta E = \Delta E(\text{orb}) + \Delta V(\text{es}) + \Delta E(\text{Pauli}) + \Delta E(\text{prep}) \quad (1)$$

Here, the $\Delta E(\text{orb})$ term accounts for the difference of the orbital energies in the complex relative to those in the isolated fragments. This term can be further broken down into $\Delta E(A1)$, $\Delta E(A2)$, and $\Delta E(E1)$ terms, which correspond to each irreducible representation in the C_{3V} point group, plus the Hartree-Fock exchange component $\Delta E(\text{XC,HF})$, which is non-local.

$$\Delta E(\text{orb}) = \Delta E(A1) + \Delta E(A2) + \Delta E(E1) + \Delta E(\text{XC,HF}) \quad (2)$$

The orbital interaction terms not only account for dative interactions between filled and unfilled orbitals (*i.e.*, the “sigma donor” charge-transfer interaction ($A1$), or “ π back-donation” ($E1$)), but also interactions between filled orbitals (which reflect polarization within the respective subunits). We note here that the $\Delta E(A2)$ terms are quite small: zero for $\text{CH}_3\text{CN}-\text{BH}_3$, and 2.0 kcal/mol or less for $\text{CH}_3\text{CN}-\text{BF}_3$ and $\text{CH}_3\text{CN}-\text{BCl}_3$. They are therefore excluded from our interpretation. The $\Delta E(\text{XC,HF})$ terms are also small, and are likewise neglected. We also note that in our most recent work,¹⁵ we included $\Delta E(\text{XC,HF})$ as a separate term in the main equation, but in keeping with more common convention we include this term in the orbital energy here. The $\Delta V(\text{es})$ term accounts for the electrostatic interactions between the subunits of the complex, prior to any electronic reorganization.

The $\Delta E(\text{Pauli})$ term is repulsive (*i.e.*, > 0), and accounts for energy changes associated with the Pauli repulsion of the electron distributions on each respective fragment upon complex formation. The other repulsive term, $\Delta E(\text{prep})$, accounts for the geometrical distortions of the donor and acceptor subunits that occur upon complex formation.

EDA analyses for $\text{CH}_3\text{CN}-\text{BCl}_3$, $\text{CH}_3\text{CN}-\text{BH}_3$, and $\text{CH}_3\text{CN}-\text{BF}_3$ at B-N distances of 1.6 and 2.9 Å (the former being near the equilibrium values of the BH_3 and BCl_3 complexes, the latter being near the long-bond equilibrium value for BCl_3) are reported in Table 2. The degrees of ionic (*% ion*) and covalent (*% cov*) character, calculated as the percentage of the sum of all attractive terms represented by $\Delta V(\text{es})$ and $\Delta E(\text{orb})$, respectively, are also reported.^{37,38}

Table 2: Energy Decomposition Parameters for $\text{CH}_3\text{CN}-\text{BX}_3$ (X = H, F, Cl)¹

Complex	$\Delta E(\text{A1})$	$\Delta E(\text{E1})$	$\Delta E(\text{prep})$	$\Delta V(\text{es})$	$\Delta E(\text{Pauli})$	$\Delta E(\text{tot})$	<i>%ion</i> ²	<i>%cov</i> ²
<i>R(B-N) = 1.6 Å</i>								
$\text{CH}_3\text{CN}-\text{BCl}_3$	-93.3	-22.1	22.6	-90.5	167.1	-5.8	44	56
$\text{CH}_3\text{CN}-\text{BH}_3$	-75.5	-15.7	12.0	-59.5	100.9	-24.3	39	61
$\text{CH}_3\text{CN}-\text{BF}_3$	-62.1	-22.6	24.1	-77.2	127.7	-4.4	48	52
<i>R(B-N) = 2.9 Å</i>								
$\text{CH}_3\text{CN}-\text{BCl}_3$	-4.2	-1.4	0.5	-4.8	5.5	-1.2	54	46
$\text{CH}_3\text{CN}-\text{BH}_3$	-6.0	0.0	0.1	-3.4	1.8	-3.3	48	52
$\text{CH}_3\text{CN}-\text{BF}_3$	-2.6	-0.4	0.4	-5.3	2.6	-3.9	71	29

1) Units of kcal/mol, and all data for structures with the B-N distance constrained to 1.6 Å to facilitate comparison between complexes. 2) % ionic ($\Delta V(\text{es})/(\Delta E(\text{A1}) + \Delta E(\text{E}) + \Delta V(\text{es}))$) and % covalent ($(\Delta E(\text{A1}) + \Delta E(\text{E})) / (\Delta E(\text{A1}) + \Delta E(\text{E}) + \Delta V(\text{es}))$) character, as defined in refs 37 & 38. See text for discussion.

At 1.6 Å, the trend in the $\Delta E(\text{A1})$ terms suggest that BCl_3 is the strongest sigma acceptor BH_3 is intermediate, and BF_3 is the weakest. Interestingly, the orbital energies calculated at the *mPW1/TZ2P* level suggest that BH_3 and BCl_3 should be comparably strong in terms of Lewis acidity,

with LUMO orbital energies (a_1) of -1.9 eV and -1.8 eV, respectively. The somewhat larger $\Delta E(A1)$ term for the $\text{CH}_3\text{CN}-\text{BCl}_3$ complex at 1.6 Å can be rationalized in that BCl_3 is presumably the most polarizable. The LUMO energy of BF_3 (+0.2 eV), however, is quite consistent with it being the weakest acceptor. We also note that the $\Delta E(E1)$ term is roughly equivalent for BF_3 and BCl_3 . The electrostatic attraction terms ($\Delta V(es)$) at 1.6 Å are sizable, and range from 39 to 48% of the total attractive terms, with the BF_3 complex being the most ionic, and the BH_3 complex the least. In comparison, all of the attractive terms are greatly reduced at 2.9 Å, especially the covalent terms. In turn, the $\Delta V(es)$ terms comprise a larger fraction of the binding energies at 2.9 Å, which is presumably reflects the greater importance of non-bonding, electrostatic interactions at longer distances.

The $\Delta E(pre)$ term is due primarily to the either hydrogen-hydrogen or halogen-halogen repulsion that occurs in the pyramidalization of the BX_3 fragment. It is therefore not surprising the $\Delta E(pre)$ term for $\text{CH}_3\text{CN}-\text{BH}_3$ is roughly half that of its halogenated analogs at 1.6 Å and is insignificant for all three complexes at 2.9 Å. The predicted trend for this term is in good qualitative agreement with reference 18, where it is discussed in detail. It also agrees qualitatively with trends observed for halogen-halogen repulsion in other systems where fluorine-fluorine interactions are found to be more strongly repulsive due to electrostatic effects.³⁸ The contributions of the nitrile fragment to the $\Delta E(pre)$ term was found to be negligible in all cases.

The $\Delta E(Pauli)$ terms differ quite significantly across the series, being largest in the case of $\text{CH}_3\text{CN}-\text{BCl}_3$ and smallest in the case of $\text{CH}_3\text{CN}-\text{BH}_3$ at both 1.6 and 2.9 Å. We have previously noted that the differences in the $\Delta E(Pauli)$ terms, when rationalized in terms of the greater repulsion between nitrile π electrons and fluorine substituents, explain the significant differences in the structural and

energetic properties of nitrile-BF₃ and -BH₃ complexes.¹⁵ In turn, we would expect greater $\Delta E(Pauli)$ contributions for CH₃CN-BCl₃. Interestingly, this trend is particularly pronounced at long B-N distances, as demonstrated graphically in Figure 7, and also in Table 2. At 2.9 Å, the attractive forces for all three complexes are comparable, but the Pauli repulsion for CH₃CN-BCl₃ is more than double that of the other complexes, resulting in roughly half the total interaction energy. Therefore, the $\Delta E(Pauli)$ term offers a compelling explanation of the topological differences in the nitrile-BX₃ potential energy surfaces. As BF₃ approaches the nitrile donor, Pauli repulsion is significant enough to dampen the attractive interactions, resulting in an unusually flat potential that is not observed for BH₃.^{4,8} However, as BCl₃ approaches the same nitrile donor, Pauli repulsion at long B-N distances is actually large enough to result in an energetic barrier, owing to the greater spatial extent of the valence orbitals of the 2nd-row halogen Cl, to prevail over the attractive interactions.

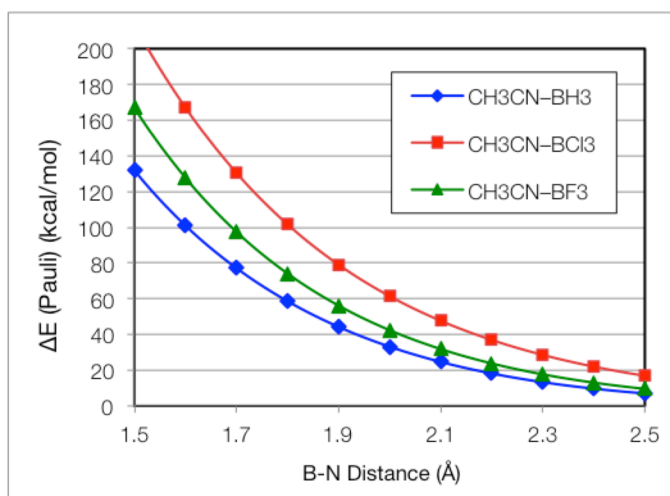


Figure 7: The distance dependence of the $\Delta E(Pauli)$ terms for CH₃CN-BF₃, CH₃CN-BCl₃ and CH₃CN-BH₃.

Conclusions

We have examined the structural and energetic properties of $\text{CH}_3\text{CN}-\text{BCl}_3$ by matrix IR spectroscopy and computational methods. Our computational analysis identified two distinct equilibrium structures of the complex. One of these, the global minimum structure, has the characteristics of a strong donor-acceptor complex, with a short B-N bond distance of 1.601 Å and a binding energy of 12.0 kcal/mol (via MP2/aug-cc-pVTZ). The other structure, a secondary minimum, exhibits characteristics of a weak, non-bonded complex, with a relatively long B-N distance 2.687 Å and a binding energy of only -4.9 kcal/mol (again via MP2/aug-cc-pVTZ). Calculated potential curves reveal that there is a significant barrier between these structures, ranging from 1-3 kcal/mol, and also that MP2/aug-cc-pVTZ binding energies are larger than those inferred from higher-level post-HF assessments of the potential. According to the CCSD/6-311+(2df,p)//MP2/6-311+(2df,p) potential curve, the global and secondary minima lie at about -7.8 and -3.6 kcal/mol relative to the energy of separated BCl_3 and CH_3CN , respectively, and that the barrier between these minima lies about 1.9 kcal/mol above the secondary minimum. Meanwhile, the CCSD(T)/6-311+(2df,p) at these key points on the potential place the global minimum at -8.5 kcal/mol, the secondary minimum at -4.0 kcal/mol, and the barrier at 1.5 kcal/mol, relative to the secondary minimum.

We were able to observe and assign several IR bands of 6 isotopic forms of $\text{CH}_3\text{CN}-\text{BCl}_3$ in solid neon. These included the BCl_3 asymmetric stretch (ν_{BCl}^a), and the CN stretch (ν_{CN}), which were observed at 792 and 2380 cm^{-1} , respectively, for the primary isotopomer ($\text{CH}_3\text{CN}-^{11}\text{BCl}_3$). Based on comparisons to *mPW1*/aug-cc-pVTZ predictions, as well as comparisons to the

measured frequencies for the solid complex, we conclude that the structure of the complex we are observing in the matrix is the “short-bond” form (i.e., global minimum) with a short B-N distance near 1.6 Å. While we did also observe frequencies near the *mPW1/aug-cc-pVTZ* predictions for the long-bond form of the complex, we conclude that these arose from CH₃CN–HCl, which forms as a result of a persistent HCl impurity in the BCl₃ sample.

Energy decomposition analyses for CH₃CN–BCl₃ and two analogous complexes, CH₃CN–BH₃ and CH₃CN–BF₃, sheds additional light on the trend in Lewis acidity of these three BX₃ species towards nitriles. Our analysis highlights the repulsion between the nitrile π density and halogen substituents on boron. This repulsion is the driving force for pyramidalization of the BX₃ fragments, which comes at an additional energetic cost for the halogenated complexes. Moreover, for larger halogen substituents, the Pauli repulsion term is also significant at longer B-N distances, which explains the barrier that occurs along the B-N potential for CH₃CN–BCl₃, as well as the extended flat region on the B-N potential for CH₃CN–BF₃.

Acknowledgements

The work was supported by the National Science Foundation grants CHE-0718164 (J.A.P.), CHE-1152820 (J.A.P.), and CHE-1229354 (MERCURY Consortium). Additional support was obtained from the Petroleum Research Fund (46291-B6 and 53066-UR6), administered by the American Chemical Society, as well as UWEC’s Office of Research and Sponsored Programs. J.A.P. also acknowledges a Henry Dreyfus Teacher-Scholar Award from the Camille and Henry Dreyfus Foundation.

References

1. N. A. Young, *Coordination Chemistry Reviews*, 2013, **257**, 956.
2. Y. Zhao and D. G. Truhlar, *Accounts of Chemical Research*, 2008, **41**, 157.
3. N. P. Wells and J. A. Phillips, *Journal of Physical Chemistry A*, 2002, **106**, 1518.
4. D. J. Giesen and J. A. Phillips, *Journal of Physical Chemistry A*, 2003, **107**, 4009.
5. J. A. Phillips, D. J. Giesen, N. P. Wells, J. A. Halfen, C. C. Knutson and J. P. Wrass, *Journal of Physical Chemistry A*, 2005, **109**, 8199.
6. J. A. Phillips, J. A. Halfen, J. P. Wrass, C. C. Knutson and C. J. Cramer, *Inorganic Chemistry*, 2006, **45**, 722.
7. A. A. Eigner, J. A. Rohde, C. C. Knutson and J. A. Phillips, *Journal of Physical Chemistry B*, 2007, **111**, 1402.
8. J. A. Phillips and C. J. Cramer, *Journal of Physical Chemistry B*, 2007, **111**, 1408.
9. A. R. Buchberger, S. J. Danforth, K. M. Bloomgren, J. A. Rohde, E. L. Smith, C. C. A. Gardener and J. A. Phillips, *Journal of Physical Chemistry B*, 2013, **117**, 11687.
10. K. R. Leopold, M. Canagaratna and J. A. Phillips, *Accounts of Chemical Research*, 1997, **30**, 57.
11. W. A. Burns and K. R. Leopold, *Journal of the American Chemical Society*, 1993, **115**, 11622.
12. M. A. Dvorak, R. S. Ford, R. D. Suenram, F. J. Lovas and K. R. Leopold, *Journal of the American Chemical Society*, 1992, **114**, 108.
13. B. Swanson, D. F. Shriver and J. A. Ibers, *Inorganic Chemistry*, 1969, **8**, 2182.
14. J. Tomasi, *Theoretical Chemistry Accounts*, 2004, **112**, 184.
15. E. L. Smith, D. Sadowsky, C. J. Cramer and J. A. Phillips, *Journal of Physical Chemistry A*, 2011, **115**, 1955.
16. F. A. Cotton and G. Wilkinson, *Advanced Inorganic Chemistry*, 5th edn., Wiley Interscience, New York, 1988.
17. T. Brinck, J. S. Murray and P. Politzer, *Inorganic Chemistry*, 1993, **32**, 2622.
18. B. D. Rowsell, F. J. Gillespie and G. L. Heard, *Inorganic Chemistry*, 1999, **38**, 4659.
19. F. Bessac and G. Frenking, *Inorganic Chemistry*, 2003, **42**, 7990.
20. V. Jonas, G. Frenking and M. T. Reetz, *Journal of the American Chemical Society*, 1994, **116**, 8741.
21. H. G. Cho and B. S. Cheong, *Journal of Molecular Structure-Theochem*, 2000, **496**, 185.
22. Cramer, C.J. *Essentials of Computational Chemistry*, 2nd edn., John Wiley and Sons, Chichester, U.K., 2004.
23. Frisch, M.J.; Trucks, G.W.; Schlegel, H.B.; Scuseria, G.E.; Robb, M.A.; Cheeseman, J.R.; Montgomery, Jr., J.A.; Vreven, T.; Kudin, K.N.; Burant, J.C. *et al.*, GAUSSIAN03 (Revision E.01), Gaussian, Inc., Wallingford CT, 2004.
24. Frisch, M.J.; Trucks, G.W.; Schlegel, H.B.; Scuseria, G.E.; Robb, M.A.; Cheeseman, J.R.; Scalmani, G.; Barone, V.; Mennucci, B.; Petersson, G.A. *et al.*, GAUSSIAN09 (Revision B.01), Gaussian, Inc., Wallingford CT, 2009.
25. J. A. Phillips and C. J. Cramer, *Journal of Chemical Theory and Computation*, 2005, **1**, 827.
26. J. F. Bertran, B. Laserna, K. Doerffel, K. Dathe and G. Kabish, *Journal of Molecular Structure*, 1982, **95**, 1.
27. K. Morokuma, *Journal of Chemical Physics*, 1971, **55**, 1236.
28. ADF2008, SCM, Theoretical Chemistry, Vrije Universiteit, Amsterdam, The Netherlands, <http://www.scm.com> SCM Inc., 2008.

29. M. Mantina, A. C. Chamberlin, R. Valero, C. J. Cramer and D. G. Truhlar, *Journal of Physical Chemistry A*, 2009, **113**, 5806.
30. B. Cordero, V. Gomez, A. E. Platero-Prats, M. Reves, J. Echeverria, E. Cremades, F. Barragan and S. Alvarez, *Dalton Transactions*, 2008, 2832.
31. D. F. Shriver and B. Swanson, *Inorganic Chemistry*, 1971, **10**, 1354.
32. Herzberg, G., *Molecular Spectra And Molecular Structure: Infrared and Raman Spectra of Polyatomic Molecules*, Krieger Publishing, Boca Raton, FL, 1989.
33. D. C. McKean and S. Machray, *Spectrochimica Acta Part A-Molecular and Biomolecular Spectroscopy*, 1988, **44**, 533.
34. D. Maillard, A. Schriver, J. P. Perchard and C. Girardet, *Journal of Chemical Physics*, 1979, **71**, 505.
35. L. Schriver, A. Schriver and J. P. Perchard, *Journal of the Chemical Society-Faraday Transactions II*, 1985, **81**, 1407.
36. F. M. Bickelhaupt and E. J. Baerends, *Reviews in Computational Chemistry, Vol 15*, 2000, **15**, 1.
37. G. Frenking, K. Wichmann, N. Frohlich, C. Loschen, M. Lein, J. Frunzke and V. M. Rayon, *Coordination Chemistry Reviews*, 2003, **238**, 55.
38. D. Sadowsky, K. McNeill and C. J. Cramer, *Environmental Science & Technology*, 2013, **47**, 14194.